Geophysica (2008), 44(1–2), 15–29

Temperature and Water Vapour Profiling by Carrier Phase GNSS Observables on Board a Radiosonde

Martin Vermeer

Helsinki University of Technology, Department of Surveying
P.O. Box 1200, FI-02015 TKK, Finland

(Received: January 2008; Accepted: March 2008)

Abstract

We propose precise, physically absolute temperature profiling based on use of radiosonde GNSS carrier phase measurements. This contribution provides some theory development, especially on error propagation both in extracting tropospheric zenith total delays and in recovering water vapour and temperature profiles from these, using an on-board precise pressure sensor. It is shown that useful precisions can be achieved even with existing technology, which holds an interest especially for meteorological and climatological research use.

Key words: radiosonde, GNSS, water vapour, temperature, profiling

1. Introduction and concept

Radiosondes are a long-established operational technique forming the backbone of the meteorological upper-air observational networks. The technique, and its error sources, are in general well understood, and it undoubtedly will remain an essential component offering *in situ* capabilities not otherwise available.

However, it is also known (e.g. *Sherwood et al.,* 2005), that measuring precise temperature on board a radiosonde can be a source of systematic error. Typically, the main purpose of these measurements has not been to provide precisely calibrated temperature values useful for, e.g., climatological studies. It would be useful though to have a technique that can do precisely that.

Note that, where it is available in the area of study, tropospheric water vapour tomography (e.g. *Champollion et al.*, 2005), while providing a three-dimensional picture of *absolute* atmospheric water vapour content, fails to give a similar spatial picture of either temperatures or *relative* humidity values. Specifically it cannot provide vertical profiles of these observables, like the technique proposed here does.

Currently the positioning, i.e., location tagging, of radiosonde measurements is often done using GNSS receivers, having become affordable and small. The measurement technique is typically based on pseudo-random noise (PRN) code correlation, providing metre-level precision, good enough for routine meteorology use.

We propose an added-value technique for temperature profiling based on use of radiosonde GNSS carrier phase measurements, which, based on existing technologies, can be of millimetre-level uncertainty. This requires use of IGS (International GNSS Service) permanent reference stations (*Dow et al*., 2005), preferably a dedicated base station at a known position near the launch site, and processing of the GNSS observations in a relative mode. Precise positioning together with barometry on an uncertainty level of 1hP or better, will allow estimation of scale heights to an uncertainty of 0.1%, providing temperature estimates of uncertainty $10^{-3} \times 300\text{K} = 0.3\text{K}$. This uncertainty would apply to height interval of 1 km; for a full scale height of 7 km, uncertainty will be even better. For weather-related use, temperatures of ±0.2–1K at vertical resolutions of 500 m to 2.5 km would be interesting; for long term climatological modelling, uncertainty could be 0.1K, e.g., for the troposphere as a whole.

The technique presupposes sufficiently good knowledge of the atmosphere's molar mass; for the dry constituents this is not a problem as these are well-mixed. For water vapour, however, we propose to use the same carrier phase observables together with those of the base station for estimating the total zenith propagation delay – containing a strong water vapour signature – above the current level of the sonde.

From this, together with ambient air pressure, the total wet delay can be derived – and local average absolute humidity follows from its vertical gradient. As water vapour refractivity is some 17 times greater than that of dry air, values thus derived will be good enough for computing the average molecular mass at the sonde's location.

Determination of temperature from scale height requires also gravity along the path of the sonde; this is not a limiting requirement, as the Earth's gravity field has been modelled to high resolution and low uncertainty.

Inexpensive GNSS sensors are available capable of measuring carrier phases, e.g., the **itrax03** from Fastrax (http://tinyurl.com/itrax03), which is already being used in Vaisala's radiosondes.

2. Zenith total delay (ZTD) precision

We know (S. Söderholm, personal comm.) that we can observe carrier phase at the double difference level to an uncertainty of $\sigma_{CP} = \pm 4$ mm using an inexpensive GPS sensor. Simultaneously estimating from such observations the zenith total delay (ZTD), receiver vertical position and receiver clock offset will inevitably lead to a much greater uncertainty in each of these derived quantities. This problem was studied by (*Vermeer*, 1997), concluding that for the vertical position co-ordinate estimate, substantial uncertainty growth occurs.

We repeat here the analysis with a focus on the uncertainty (standard deviation) of the total tropospheric zenith delay unknown.

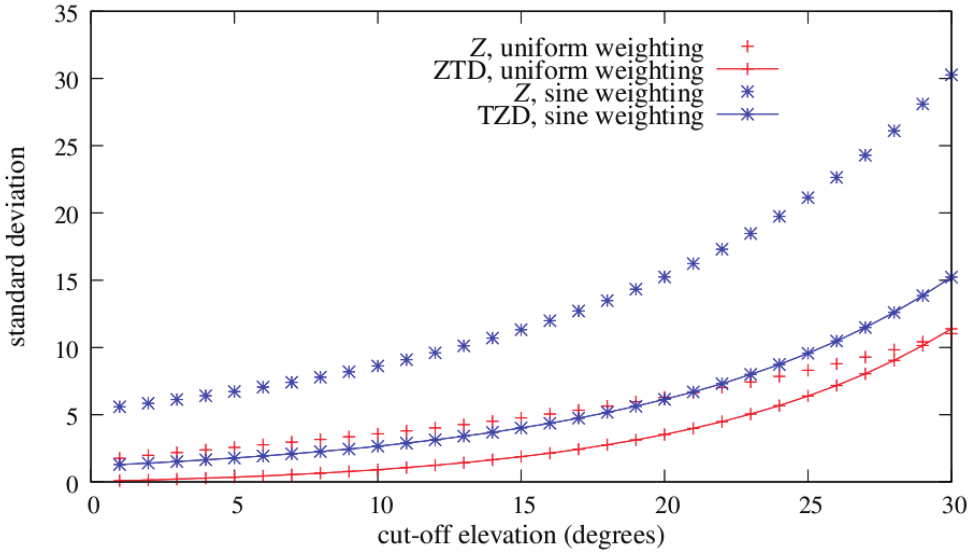

Fig. 1. Standard deviation of the vertical position co-ordinate Z and the tropospheric zenith delay ZTD, respectively. The values plotted correspond to a single pseudo-range observation precision of 1 and a number of visible satellites of 2π, and should thus be scaled for true precision and number of satellites.

We start from the same observation equations, where the unknowns are numbered 1…3 for the co-ordinates X,Y,Z (with Z pointing upward), 4 the receiver clock unknown, and 5 the tropospheric zenith delay unknown. With this, the corresponding elements in the design matrix become

$$\begin{aligned} a_1(z,A) &= \sin z \sin A, \\ a_2(z,A) &= \sin z \cos A, \\ a_3(z,A) &= \cos z, \\ a_4(z,A) &= 1, \\ a_5(z,A) &= (\cos z)^{-1}. \end{aligned} \tag{1}$$

Here, z and A are zenith angle and azimuth, respectively.

As in the referred paper, we compute the elements of the normal matrix by integration over that part of the celestial sphere, σ_0, where satellites are visible:

$$n_{ij} = \iint_{\sigma_0} a_i(z,A)\, a_j(z,A)\, p(z)\, d\sigma, \tag{2}$$

where i,j are the two distinct unknowns that we wish to estimate. Both subscripts are in the interval 1…5.

For $p(z)$, the weight function, we consider two alternatives[1]

[1] Note that both imply that the probability density for satellites is independent of azimuth. The assumption of azimuthal symmetry and the even distribution of satellites over a cap as a means of simplifying GPS error analysis can already be found in (*Sjöberg*, 1992), who also refers to (*Beutler et al.*, 1988) and (*Geiger*, 1987); something the author and reviewers of (*Vermeer*, 1997) were apparently unaware of.

1. Uniform weighting: $p(z) = 1$
2. Sine weighting: $p(z) = \cos^2 z$.

we also assume that the integration cap σ_0 is the area above the zenith angle z_0 for which $\cos z_0 = s$. Then we may write

$$\begin{aligned} n_{ij} &= \int_0^{z_0}\int_0^{2\pi} a_i(z,A)\, a_j(z,A)\, p(z)\, dA \sin z dz = \\ &= \int_s^1\int_0^{2\pi} a_i(t,A)\, a_j(t,A)\, p(t)\, dA dt, \end{aligned} \tag{3}$$

where $t = \cos z$.

The integration over A using Eqs. (1) yields for the full 5 × 5 normal matrix:

$$N = 2\pi\int_s^1 \begin{bmatrix} \frac{1}{2}(1-t^2) & & & & \\ & \frac{1}{2}(1-t^2) & & & \\ & & t^2 & t & 1 \\ & & t & 1 & t^{-1} \\ & & 1 & t^{-1} & t^{-2} \end{bmatrix} p(t)\, dt. \tag{4}$$

For the case of *uniform weighting* $p(t) = 1$ we obtain

$$\begin{aligned} N &= 2\pi \begin{bmatrix} \frac{1}{2}t - \frac{1}{6}t^3 & & & & \\ & \frac{1}{2}t - \frac{1}{6}t^3 & & & \\ & & \frac{1}{3}t^3 & \frac{1}{2}t^2 & t \\ & & \frac{1}{2}t^2 & t & \ln t \\ & & t & \ln t & -t^{-1} \end{bmatrix}\Bigg|_s^1 = \\ &= 2\pi \begin{bmatrix} n_{11} & & & & \\ & n_{22} & & & \\ & & \frac{1}{3} - \frac{1}{3}s^3 & \frac{1}{2} - \frac{1}{2}s^2 & 1-s \\ & & \frac{1}{2} - \frac{1}{2}s^2 & 1-s & -\ln s \\ & & 1-s & -\ln s & s^{-1} - 1 \end{bmatrix}, \end{aligned} \tag{5}$$

with $n_{11} = n_{22} = \frac{1}{3} - \frac{1}{2}s + \frac{1}{6}s^3$. From this, we derive formulas for elements of the inverse matrix N^{-1} using the `maxima` symbolic algebra package (*Anon*, 2008):

$$\left(N^{-1}\right)_{33} = \frac{1}{2\pi}\frac{-12\left(s\ln^2 s-(s-1)^2\right)}{\left(\begin{array}{l}4s\left(s^2+s+1\right)\ln^2 s-\\ -12s(s-1)(s+1)\ln s-\\ -(s-1)^2\left(s^2-14s+1\right)\end{array}\right)}; \tag{6}$$

$$\left(N^{-1}\right)_{55} = \frac{1}{2\pi}\frac{(s-1)^3 s}{\left(\begin{array}{l}4s\left(s^2+s+1\right)\ln^2 s-\\ -12s(s-1)(s+1)\ln s-\\ -(s-1)^2\left(s^2-14s+1\right)\end{array}\right)}. \tag{7}$$

For the case of *sine weighting*, we similarly obtain, skipping intermediate steps

$$N = 2\pi\int_s^1 \begin{bmatrix} \frac{1}{2}\left(1-t^2\right) & & & & & \\ & \frac{1}{2}\left(1-t^2\right) & & & & \\ & & & t^2 & t & 1 \\ & & & t & 1 & t^{-1} \\ & & & 1 & t^{-1} & t^{-2} \end{bmatrix} t^2 dt =$$

$$= 2\pi\begin{bmatrix} n_{11} & & & & & \\ & n_{22} & & & & \\ & & \frac{1}{5}\left(1-s^5\right) & \frac{1}{4}\left(1-s^4\right) & \frac{1}{3}\left(1-s^3\right) & \\ & & \frac{1}{4}\left(1-s^4\right) & \frac{1}{3}\left(1-s^3\right) & \frac{1}{2}\left(1-s^2\right) & \\ & & \frac{1}{3}\left(1-s^3\right) & \frac{1}{2}\left(1-s^2\right) & 1-s & \end{bmatrix}, \tag{8}$$

gain with $n_{11} = n_{22} = \frac{1}{15} - \frac{1}{6}s^3 + \frac{1}{10}s^5$. For this case, `maxima` gives us:

$$\left(N^{-1}\right)_{33} = \frac{1}{2\pi}\frac{180}{(1-s)^5}; \tag{9}$$

$$\left(N^{-1}\right)_{55} = \frac{1}{2\pi}\frac{9(s+1)^4}{(1-s)^5}. \tag{10}$$

The derived functions, for observable 3 – vertical co-ordinate – and observable 5 – tropospheric zenith delay – were plotted (after square rooting them to obtain standard deviations) in Figure 1.

We see that using sine weighting leads to a clear deterioration of the vertical co-ordinate estimates. This could be expected, but nevertheless sine weighting is to be

recommended as being a more realistic description of the true behaviour of measurement precision. Note that in all these computations, we assume the weighting function $p(z)$ to represent true measurement precision. Based on experience however, this is a realistic assumption only for sine weighting.

For the zenith total delays, we see that they have on the whole a considerably smaller standard deviation than than vertical co-ordinates, especially for low cut-off angles. This applies especially for uniform weighting, which appears even to go to zero for zero cut-off angle, which is undoubtedly not physical. Anyway, uniform weighting is not to be recommended.

The choice of cut-off angle is a balancing act between the wish to recover tropospheric zenith delays of low uncertainty, requiring a well-conditioned observation geometry and thus a low cut-off angle, and the reality of a not precisely horizontally stratified troposphere (the assumption underlying the whole method) affecting the results less for horizontally less extended air volumes, i.e., higher cut-off angles. For a commonly used cut-off angle like 20º and sine weighting, we see a deterioration factor for zenith total delays of six times, i.e.,

$$\sigma_d \approx 6 \cdot \sigma_{\mathrm{CP}}. \tag{11}$$

For the above mentioned σ_{CP} this would mean for the standard deviation of the total tropospheric zenith delay: $\sigma_d = \pm 24\,\mathrm{mm}$.

3. *The refractivity of air*

We can express the microwave refractive index as (*Rueger*, 2002):

$$N_M = (n_M - 1) \cdot 10^6 = \frac{K_1'}{T}\left(p - e - p_{\mathrm{CO}_2}\right) + \frac{K_2}{T} e + \frac{K_3}{T^2} e + \frac{K_4}{T} p_{\mathrm{CO}_2}, \tag{12}$$

where p and e are air pressure and water vapour partial pressure, respectively, in hPa, p_{CO_2} is carbon dioxide partial pressure, and T is temperature in Kelvin. Current best values quoted by Rueger are $K_1' = 77.6681\ \mathrm{K\,hPa^{-1}}, K_2 = 71.2952\ \mathrm{KhPa^{-1}}, K_3 = 375463\ \mathrm{K^2 hPa^{-1}}$ and $K_4 = 133.4800\ \mathrm{K\,hPa^{-1}}$.

Rueger believes dry refractivity (refractivity associated with dry air partial pressure, i.e., the K_1' and K_4 terms together) computed with this formula to be good to ±0.02% and wet refractivity (the K_2 and K_3 terms together) good to ±0.2%. The formula is intended for the 1 Hz to 1 GHz frequency range; the frequencies used by GPS lie slightly outside this range.

Substituting the value

$$p_{\mathrm{CO}_2} = 380 \cdot 10^{-6}\,(p - e) \tag{13}$$

yields the specialized equation

$$N_M = (n_M - 1)\cdot 10^6 = \frac{K_1}{T}(p - e) + \frac{K_2}{T}e + \frac{K_3}{T^2}e, \tag{14}$$

where the dry refractivity coefficient is

$$\begin{aligned} K_1 &= K_1' + (K_4 - K_1')\frac{p_{CO_2}}{p - e} = \\ &= 77.6681\ \mathrm{K\,hPa^{-1}} + 55.8119\ \mathrm{K\,hPa^{-1}}\cdot 380\cdot 10^{-6} = \\ &= 77.6893\ \mathrm{K\,hPa^{-1}}. \end{aligned} \tag{15}$$

The "good to 0.02%", applied to this coefficient, means ±0.0155 K hPa^{-1}, so the last stated digits are meaningless. A similar attribution for the wet refractivity coefficients cannot be made as readily, as there are two of them, K_2 and K_3. Attributing all uncertainty to the dominant K_3 yields for the stated ±0.2% uncertainty: $K_3 = 375463 \pm 751\ \mathrm{K^2hPa^{-1}}$.

Table 1. Concentrations of gases and their molecular masses, according to (*Williams*, 2008). Note that the percentage sum exceeds 100%, even though some rare species are not included here. *The CO_2 concentration is in reality time dependent.

Species	Concentration (%)	Molecular mass (g/mol)	Contrib.
N_2	78.084	28.0134	21.8740
O_2	20.946	31.9988	6.7024
Ar	0.9340	39.948	0.3731
CO_2	0.0380*	44.01	0.0167
Ne	0.001818	20.2	0.0004
	100.003818	Total (M_{dry})	28.9666
	100	Adjusted to 100%	28.9655

4. The mean molecular mass of air

The air's mean molecular mass is the weighted mean of that of dry air and that of water vapour, the masses being the partial pressures $p - e$ and e. The formula for *scale height* is

$$S = \frac{RT}{Mg} \tag{16}$$

where M is the mean molar mass:

$$M = \frac{p - e}{p}M_{dry} + \frac{e}{p}M_{H_2O}. \tag{17}$$

Table 1 (*Williams*, 2008) gives concentrations of gases and their molecular masses.

For water vapour, we use $M_{\mathrm{H_2O}} = 18.0$. The concentration of CO_2 is slowly increasing; 380 ppmv was around 2007. The effect of this on mean molecular mass is hard to calculate very precisely, as the amount of O_2 removed depends somewhat on the mix of carbon and hydrogen in the organic substances whose oxydation is causing the increase.

5. *Zenith delay and pressure*

We may assume that the measured total zenith delay, in metric units, is the following integral:

$$d_0(H) - d_0(0) = -10^{-6} \int_0^H N_M \, dH'. \tag{18}$$

Substituting the expression (Eq. 14) for N_M, we obtain

$$d_0(H) - d_0(0) = -10^{-6} \int_0^H \left\{ \frac{K_1}{T} p + \left[\frac{K_2 - K_1}{T} + \frac{K_3}{T^2} \right] e \right\} dH'. \tag{19}$$

This is an *observation equation*, where $d_0(H) - d_0(0)$ is the observed quantity, and e and T are unknowns.

If we assume that also the air pressure p is measured at known heights (GPS), we get additionally

$$\begin{aligned} p(H) - p(0) &= \int_{p(0)}^{p(H)} dp' = \\ &= -\int_0^H \frac{p}{S} dH' \\ &= -\int_0^H M \frac{gp}{RT} dH' = \\ &= -\frac{1}{R} \int_0^H \left(pM_{\mathrm{dry}} + e\left[M_{\mathrm{H_2O}} - M_{\mathrm{dry}} \right] \right) \frac{g}{T} dH'. \end{aligned} \tag{20}$$

This is a second observation equation.

Note that the function $p\,(H)$ is considered directly measured. This means that the Eqs. (19, 20) could be directly solved stepwise from the ground up to obtain $e\,(H)$ and $T\,(H)$.

6. *Error propagation analysis*

What interests us here is the error propagation behaviour when calculating $e(H)$ and $T(H)$ using Eqs. (19, 20). For this we have to linearize. We find for the linear dependencies:

$$\Delta d_0 \approx -10^{-6} K_1 \int_0^H \Delta\left(\frac{p}{T}\right) dH' - 10^{-6} K_3 \int_0^H \Delta\left(\frac{e}{T^2}\right) dH', \tag{21}$$

$$\Delta p \approx -\frac{\overline{g}}{R} M_{\mathrm{dry}} \int_0^H \Delta\left(\frac{p}{T}\right) dH' - \\ -\frac{\overline{g}}{R}\left[M_{\mathrm{H_2O}} - M_{\mathrm{dry}}\right] \int_0^H \Delta\left(\frac{e}{T}\right) dH', \tag{22}$$

where in the first we have retained only the dominant K_1, K_3 terms, and in the second considered g known – replaced by an average over the interval of integration.

Executing the linearization now produces:

$$\Delta d_0 \approx +10^{-6} K_1 \frac{1}{T_0^2} \int_0^H p \Delta T \, dH' - \\ -10^{-6} K_3 \left[\frac{1}{T_0^2} \int_0^H \Delta e \, dH' - \frac{2e_0}{T_0^3} \int_0^H \Delta T \, dH'\right], \tag{23}$$

$$\Delta p \approx +\frac{\overline{g}}{R} M_{\mathrm{dry}} \frac{1}{T_0^2} \int_0^H p \Delta T \, dH' - \\ -\frac{\overline{g}}{R}\left[M_{\mathrm{H_2O}} - M_{\mathrm{dry}}\right]\left[\frac{1}{T_0} \int_0^H \Delta e \, dH' - \frac{e_0}{T_0^2} \int_0^H \Delta T \, dH'\right]. \tag{24}$$

Here, e_0, T_0 etc. are the reference or approximate values used in the linearization.

Now by the substitutions of integrated values

$$\overline{\Delta e} = \int_0^H \Delta e dH', \tag{25}$$

$$\overline{p\Delta T} = \int_0^H p \Delta T dH', \tag{26}$$

this becomes

$$\Delta d_0 \approx +10^{-6} K_1 \frac{1}{T_0^2} \overline{p\Delta T} - 10^{-6} K_3 \left[\frac{1}{T_0^2} \overline{\Delta e} - \frac{2e_0}{T_0^3} \int_0^H \Delta T \, dH'\right], \tag{27}$$

$$\Delta p \approx +\frac{\overline{g}}{R} M_{\mathrm{dry}} \frac{1}{T_0^2} \overline{p\Delta T} -$$

$$-\frac{\overline{g}}{R}\left[M_{\mathrm{H_2O}} - M_{\mathrm{dry}}\right]\left[\frac{1}{T_0}\overline{\Delta e} - \frac{e_0}{T_0^2}\int_0^H \Delta T\, dH'\right]. \tag{28}$$

Substitute numerical values into this: $K_1 = 77.6893$ K hPa^{-1}, $K_3 = 375463$ K^{2}hPa^{-1}, $R = 8314$ J K^{-1} kmol^{-1}, $\overline{g} = 9.8$ m s^{-2}, $T_0 = 288$ K, $e_0 = 0$. Then

$$\Delta d_0 = +9.37\cdot10^{-10}\,\mathrm{K^{-1}hPa^{-1}}\cdot\overline{p\Delta T} - 4.527\cdot10^{-6}\,\mathrm{hPa^{-1}}\cdot\overline{\Delta e} =$$

$$= +9.37\cdot10^{-12}\,\mathrm{K^{-1}Pa^{-1}}\cdot\overline{p\Delta T} - 4.527\cdot10^{-8}\,\mathrm{Pa^{-1}}\cdot\overline{\Delta e}, \tag{29}$$

$$\Delta p = +4.12\cdot10^{-7}\,\mathrm{K^{-1}m^{-1}}\cdot\overline{p\Delta T} + 4.49\cdot10^{-5}\,\mathrm{m^{-1}}\cdot\overline{\Delta e}. \tag{30}$$

This is good enough for error propagation.

We must use S.I. units m, s, K, and Pa throughout, necessitating the above unit conversion.

Write this in matrix form:

$$\begin{bmatrix}\Delta d_0\\ \Delta p\end{bmatrix} = \begin{bmatrix}+9.37\cdot10^{-12} & -4.527\cdot10^{-8}\\ +4.12\cdot10^{-7} & +4.49\cdot10^{-5}\end{bmatrix}\begin{bmatrix}\overline{p\Delta T}\\ \overline{\Delta e}\end{bmatrix}. \tag{31}$$

The inverse system is

$$\begin{bmatrix}\overline{p\Delta T}\\ \overline{\Delta e}\end{bmatrix} = \begin{bmatrix}+2.3542\cdot10^{9} & +2.3736\cdot10^{6}\\ -2.1602\cdot10^{7} & +4.9130\cdot10^{2}\end{bmatrix}\begin{bmatrix}\Delta d_0\\ \Delta p\end{bmatrix} \tag{32}$$

This equation can be used for propagation of variances. For typical values[2] $\sigma_d = \pm 0.024$ m and $\sigma_p = \pm 100$ Pa we obtain in this way a variance matrix

$$\mathrm{Var}\begin{pmatrix}\overline{p\Delta T}\\ \overline{\Delta e}\end{pmatrix} = \begin{bmatrix}5.9534\cdot10^{16} & -1.7632\cdot10^{13}\\ -1.7632\cdot10^{13} & 2.7121\cdot10^{11}\end{bmatrix}. \tag{33}$$

This yields

$$\sigma_{\overline{p\Delta T}} = \pm 2.44\cdot10^{8}\ \mathrm{K\ Pa\ m}, \tag{34}$$

$$\sigma_{\overline{\Delta e}} = \pm 52078\ \mathrm{Pa\ m}. \tag{35}$$

[2] Note that, as described by Eqs. (19, 20), these standard deviations refer to *differences* of tropospheric zenith delays and air pressures over a height interval.

The *a posteriori* correlation between the two unknowns amounts to –14% in this example case.

7. Interpretation

Note that in the previous section, the estimated quantities $\overline{p\Delta T}$ and $\overline{\Delta e}$, as well as their mean errors, are actually integrated quantities, representing temperature deviation and the deviation of the partial pressure of water vapour integrated over a height interval. In the derivation, the height interval was taken as $[0, H]$, but it could be any height interval. For a small interval it is correct, as we have done, to move g outside the integral and replace it by its average over the height interval considered.

Obviously the uncertainty of estimation of temperature and humidity will depend on the size of the height interval considered. For temperature estimation also the pressure p over the interval matters.

Near ground level (1013 hPa = 101300 Pa), for a height interval of 1000 m, we will be able to estimate the mean temperature deviation with a standard deviation of

$$\begin{aligned} \sigma_T &\approx \frac{\sigma_{\overline{p\Delta T}}}{\Delta H \cdot p} = \\ &= \pm\frac{2.3736 \cdot 10^8}{1000 \cdot 101300}\,\mathrm{K} \approx \\ &\approx \pm 2.4\,\mathrm{K}, \end{aligned} \tag{36}$$

and the mean partial pressure of water vapour with a standard deviation

$$\begin{aligned} \sigma_e &\approx \frac{\sigma_{\overline{\Delta e}}}{\Delta H} = \\ &= \frac{49402}{1000}\,\mathrm{Pa} \approx \\ &\approx \pm 0.5\,\mathrm{hPa}. \end{aligned} \tag{37}$$

The uncertainty of the temperature estimate will grow with height due to the smaller pressure p to divide by.

8. Error simulations

Numerical experimentation (see Figs. 2, 3, 4) shows some interesting things concerning the behaviour of the standard deviation values for temperature and partial water vapour pressure depending on the assumed standard deviation of air pressure σ_p and that of the zenith total delay σ_d. It appears that temperature estimates depend critically on both pressure and ZTD measurement standard deviation in the range considered, while water vapour uncertainty depends only on the ZTD measurement

uncertainty for pressure measurements of uncertainty better than ±1 hPa. Only for pressure measurements of greater uncertainty, a dependency develops.

As an example of the state of the art is Vaisala's BAROCAP® (*Vaisala Oyj*, 2008) it offers a resolution of 0.1 hPa, and a stated "reproducibility in sounding[3]" of 0.5 hPa for pressure levels of 1080 – 100 hPa, and 0.3 hPa for levels of 100 – 3 hPa.

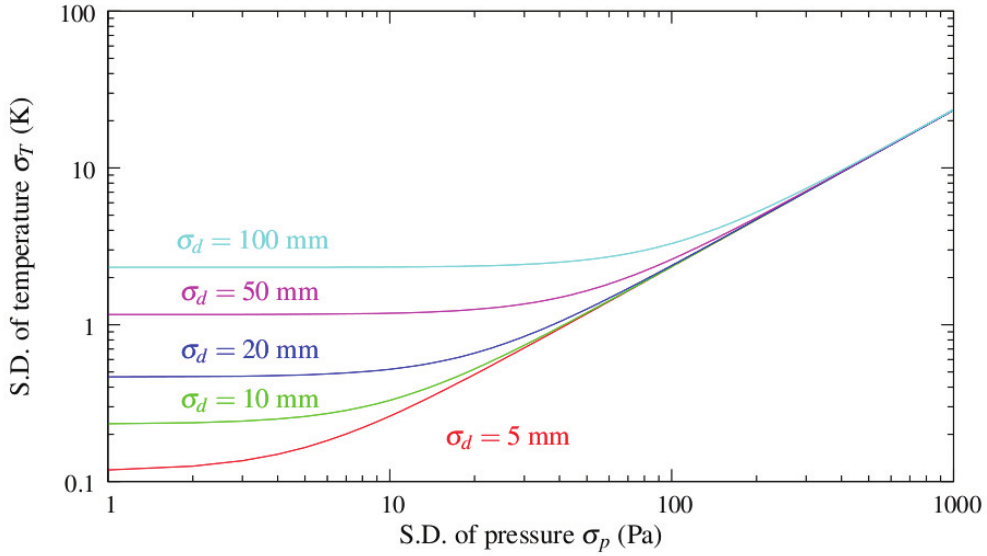

Fig. 2. Temperature precision σ_T depending on assumed σ_p and σ_d. 1 km layer, sea level pressure.

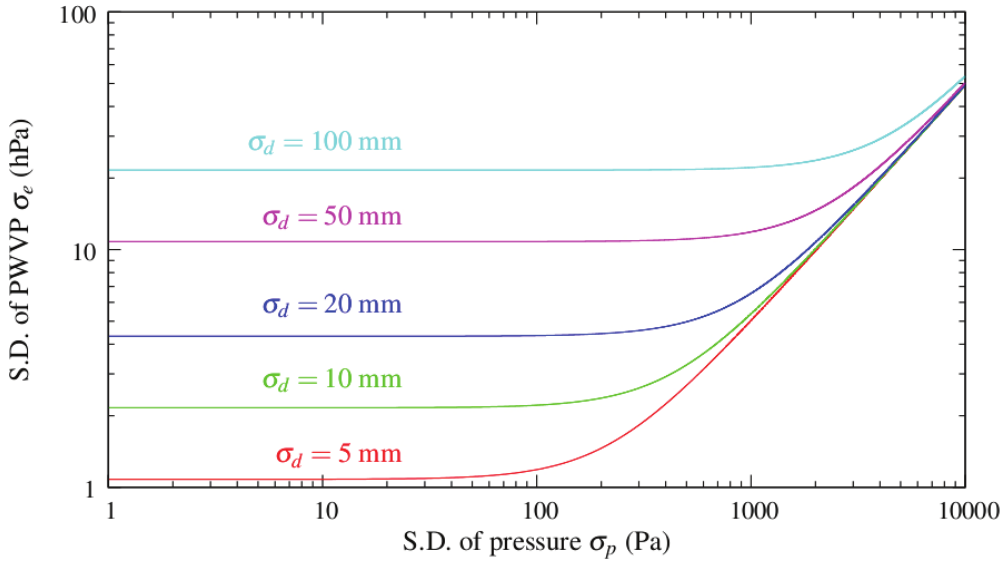

Fig. 3. Water vapour precision σ_e depending on assumed σ_p and σ_d. 1 km layer, sea level pressure.

9. Discussion and conclusions

A temperature uncertainty of ±2 K may seem poor, but note the assumed height interval of 1000 m. Over 5000 m one would already obtain sub-Kelvin uncertainty, and

[3] Defined as "standard deviation of differences, in twin soundings".

this is a currently available, inexpensive technology. Also, a pressure sensor uncertainty of ±1 hPa is conservative. A good approach would be to divide the tropophere up in layers, compute the temperature value for each of them, and then aggregated values of lower uncertainty for the whole troposphere.

9.1 Problems

1. Inexpensive receivers as used in radiosondes provide only L_1 frequency carrier phases. Ionosphere modelling, needed to be able to use single-frequency receivers on board the sonde, can be done using the global tracking network of the IGS (*Dow et al*. 2005) and ideally also the base station, which then should be dual frequency. Successfully eliminating the effect of ionospheric refraction from the estimates of tropospheric zenith delay requires careful analysis.
2. Unless atmospheric conditions are stable, the hydrostatic equilibrium assumption needed for applying the above theory will not be valid. Measurements should thus not be undertaken, or not be relied upon, e.g, under conditions of front passage, high winds, or active convection.
3. The sonde will be carried by air currents to horizontal locations away from the launch site. This may lead to a need to account for the horizontal gradient of air pressure. However, wind velocities typically are perpendicular to air pressure gradients, which should limit the size of this effect. On the other hand, in baroclinic regions, wind direction changes with height.
4. Care should be taken to avoid multipath, by properly designing the antenna mount. One possibility is mounting both ground station and radiosonde antennas on the ends of long beams. Both antennas should be electrically identical, or the phase delay patterns of both carefully calibrated. The pendular motion of the payload after launch is another problem to be addressed.
5. While the above theory tells that a low elevation cut-off is desirable, this has drawbacks: the temperature and water vapour profiles derived will then apply to a very large area around the trajectory of the sonde, where the assumption of a horizontally layered atmosphere becomes progressively less valid.

9.2 Benefits

Climatology: A major *advantage* of the technique is that it is directly based on the simple physics of the scale height, like also, e.g., GNSS limb sounding. The scale height of a gas in hydrostatic equilibrium is an absolute thermometer not needing calibration. GPS limb sounding, especially in the tropics where the atmosphere contains a lot of water vapour, cannot be used all the way down to sea level, and thus the proposed technique would be complementary if adopted worldwide. Long term climate monitoring is critically dependent upon the stability of the measurement processes being used.

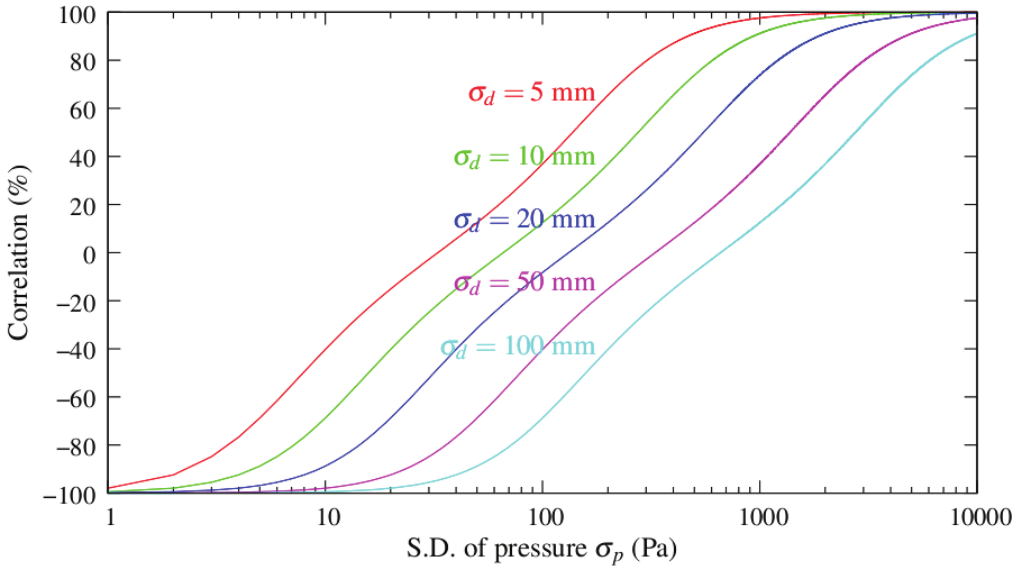

Fig. 4. Correlation between temperature and partial water vapour pressure estimators; 1 km layer, sea level pressure.

Meteorology: From the saturation water vapour pressure equation

$$e = 6.112 \exp \frac{17.67t}{243.5^{\circ}\mathrm{C} + t} \mathrm{hPa} \tag{38}$$

one can show by substitution (t = 0 – 40ºC) that an error of 1ºC in measuring temperature t produces a 7.5 – 5.5% error in partial water vapour pressure for a given relative humidity. This represents a lot of latent heat, especially in the tropics. The proposed method circumvents the problem by deriving the temperatures from the water vapour. Note that the situation for absolute measurement of water vapour profiles by radiosonde has not been any better really than that for temperatures, see, e.g., (*Szczodrak et al*., 2005). More precise profiles (of actual water vapour content) might help produce better understanding, and better predictions, in the long run. Radiosondes are a technique that can be used to calibrate and validate other techniques.

Acknowledgements

Useful discussions with Stefan Söderholm of Fastrax Oy; inspiration to do something useful related to climatology by the good folks at http://realclimate.org. Two thorough reviewers contributed materially to the correctness and clarity of the paper.

References

Anon. 2008. Maxima, a computer algebra system. URL: http://maxima.sourceforge.net/. Accessed Jan. 9, 2008.

Beutler, G., I. Bauersima, W. Gurtner, M. Rothacher, T. Schildknecht and A. Geiger, 1988. Atmospheric refraction and other important biases in GPS carrier phase observations. In F. Brunner (Ed.), *Atmospheric Effects on Geodetic Space Measurements*, number 12 (pp. 15–43). School of Surveying, University of New South Wales.

Champollion, C., F. Masson, M.-N. Bouin, A. Walpersdorf, E. Doerflinger, O. Bock and J.V. Baelen, 2005. Baelen, GPS water vapour tomography: preliminary results from the ESCOMPTE field experiment. *Atmospheric Research*, **74**(1–4), 253–274. DOI: 10.1016/j.atmosres.2004.04.003.

Dow, J.M., R.E. Neilan, and G. Gendt, 2005. The International GPS Service (IGS): Celebrating the 10th Anniversary and Looking to the Next Decade. *Adv. Space Res.*, **36**(3), 320–326. DOI: 10.1016/j.asr.2005.05.125.

Geiger, A. 1987. Simplified error estimation of positioning. In J.P. Laboratory (Ed.), *GPS Technology Workshop* Pasadena.

Rueger, J.M. 2002. Refractive Index Formulae for Radio Waves. In *FIG XXII International Congress, Washington DC, April 19–26, 2002*.

Sherwood, S.C., J.R. Lanzante and C.L. Meyer, 2005. Radiosonde Daytime Biases and Late-20th Century Warming. *Science*, **309**(5740), 1556–1559. DOI: 10.1126/science.1115640.

Sjöberg, L.E. 1992. Systematic tropospheric errors in geodetic positioning with the global positioning system. *manuscripta geodaetica*, **17**, 201–209.

Szczodrak, M., P.J. Minnett, and C. Gentemann, 2005. Long Term Comparison of AMSR-E Retrievals and Ship Based Measurements of Total Water Vapor in the Caribbean Sea. *AGU Fall Meeting Abstracts*, (pp. B907+).

Vaisala Oyj, 2008. Vaisala radiosonde RS92-KL (datasheet). http://www.jo.zan.hu/reklam/radiosonde/radiosonde.pdf. Accessed April 22, 2008.

Vermeer, M. 1997. The precision of geodetic GPS and one way of improving it. *Journal of Geodesy*, **71**, 240–245.

Williams, D.R. 2008. Earth Fact Sheet. http://nssdc.gsfc.nasa.gov/planetary/factsheet/earthfact.html. Accessed Jan. 7, 2008.